Mapping Heat Origin in Plasmonic Structures

Guillaume Baffou,[1,*] Christian Girard,[2] and Romain Quidant[1,3,†]

[1]*ICFO-Institut de Ciències Fotòniques, Mediterranean Technology Park, 08860 Castelldefels (Barcelona), Spain*
[2]*CEMES, CNRS, Université Paul Sabatier, 29 rue J. Marvig, F-31055 Toulouse, France*
[3]*ICREA-Institució Catalana de Recerca i Estudis Avançats, 08010 Barcelona, Spain*

We investigate the physics of photoinduced heat generation in plasmonic structures by using a novel thermal microscopy technique based on molecular fluorescence polarization anisotropy. This technique enables us to image the heat source distribution in light-absorbing systems such as plasmonic nanostructures. While the temperature distribution in plasmonic nanostructures is always fairly uniform because of the fast thermal diffusion in metals, we show that the heat source density is much more contrasted. Unexpectedly the heat origin (thermal hot spots) usually does not correspond to the optical hot spots of the plasmon mode. Numerical simulations based on the Green dyadic method confirm our observations and enable us to derive the general physical rules governing heat generation in plasmonic structures.

PACS numbers: 73.20.Mf, 33.50.−j, 44.10.+i

Gold nanoparticles can efficiently absorb visible or infrared light energy in very confined volumes, making them ideal remotely controllable nanosources of heat. Besides the fundamental interest of understanding nanothermodynamics phenomena, the ability to produce pointlike heat sources opens up a wide range of applications in physics, chemistry, and biology. For instance, gold nanoparticles as nanosources of heat already have promising applications in nanoscale catalysis [1], magnetism [2], microfluidics [3–5], phononics [6,7], and medicine [8–11], such as for photothermal cancer cell destruction or drug delivery. However, while the physics of thermal radiative transfer in plasmonics has been widely studied, mostly by Greffet and co-workers [12–14], the physics of heat generation and thermal diffusion in plasmonic nanostructures is poorly investigated and understood mostly due to the lack of experimental tools.

In this Letter, we investigate experimentally the physics of heat generation in gold plasmonic nanostructures by using a novel thermal microscopy technique. Based on fluorescence polarization anisotropy, this technique enables us to map the heat source density within arbitrarily complex plasmonic structures upon laser illumination with a resolution of about 300 nm. We apply this method to two different geometries: an elongated gold nanowire and a gold nanorod dimer. We show that the spatial origin of heat in the metal does not usually match the optical near-field distribution. Simulations based on the Green dyadic technique are performed to validate our experimental data and gain further understanding of the involved physics. Finally, as a direct application of our method, we show that nanohole patterning is an efficient way to enhance heat generation in metals.

Let us consider a plasmonic metal structure embedded in a condensed (fluid or solid) medium. In the steady state regime, the heating processes inside and outside plasmonic structures are governed by the Poisson equation [15]:

$$\kappa \nabla^2 T(\mathbf{r}) = -h(\mathbf{r}), \qquad (1)$$

where κ is the thermal conductivity (either of the metal or the surroundings), $T(\mathbf{r})$ is the temperature distribution, and $h(\mathbf{r})$ represents the heat source density (HSD) that has dimensions of a power per unit volume. For submicrometric metal structures heated by external illumination, the HSD $h(\mathbf{r})$ can be strongly nonuniform, depending on the morphology of the metal structure [16]. However, despite the nonuniformity of the heat origin $h(\mathbf{r})$, the temperature $T(\mathbf{r})$ remains quasiuniform throughout the metal due to the very high thermal conductivity of metals compared with that of the surroundings. For instance, the ratio between thermal conductivity of gold and water reaches about 500. As a consequence, thermal characterization restricted to the steady temperature distribution $T(\mathbf{r})$ lacks important information compared with the heat origin $h(\mathbf{r})$ inside the structure [17].

The novel thermal imaging method presented in this study is based on measuring the fluorescence polarization anisotropy (FPA) of fluorophores dispersed in solution. Briefly, a temperature increase tends to make the fluorescent molecules rotate faster during their fluorescence lifetime, which consequently reduces the degree of polarization of the emitted fluorescence. In an earlier study we showed that FPA measurements provide direct information on the distribution of the steady temperature $T(\mathbf{r})$ [17]. In this work, using a dual-objective setup and different illumination and scanning conditions, the technique has been further developed to assess the HSD $h(\mathbf{r})$, a quantity that provides much more information than only the knowledge of the temperature distribution $T(\mathbf{r})$.

The samples consist of gold nanostructures made by e-beam lithography, lying upon glass and surrounded by a glycerol-water (4:1) mixture in which fluorescein molecules are dispersed. The use of glycerol instead of pure water is intended to slow down the rotational motion of the

molecules to increase the sensitivity of the method. Figure 1 presents the setup that we used to perform both thermal (temperature and HSD) and optical (two-photon luminescence of gold) measurements. It comprises two illumination parts: a blue laser beam (473 nm) from the bottom of the sample to excite the fluorescent molecules and an infrared (IR) laser beam from the top of the sample. This IR laser beam can be tuned between 700 and 900 nm and switched from cw to pulsed mode. The cw mode is used to heat the plasmonic structures while the pulsed mode is used for the two-photon luminescence (TPL) measurements. Using two fast steering mirrors, both laser beams can be individually positioned and eventually raster scanned. The sample is mounted on a piezostage that can be raster scanned as well. All these degrees of freedom allow us to assess different physical quantities by scanning either the blue beam, the infrared beam, or the sample. To obtain the steady state temperature map $T(\mathbf{r})$, the metal structure of interest is illuminated by an extended (unfocused) IR light through the upper objective, the sample stage is fixed, and the bottom blue beam is raster scanned throughout the sample. Conversely, to measure the HSD, the blue beam and the IR beam are both focused and spatially overlapped while the stage is scanned. In such a configuration, local heating and FPA probing are performed simultaneously at each scan location. In the following, we first demonstrate that the HSD is indeed the physical quantity measured when using the later illumination and scanning conditions.

In a metal and, in particular, in a plasmonic structure under illumination, the HSD arises from Joule effect [16]:

$$h(\mathbf{r}) = \frac{1}{2}\{\mathbf{j}^\star(\mathbf{r}) \cdot \mathbf{E}(\mathbf{r}) + \mathbf{j}(\mathbf{r}) \cdot \mathbf{E}^\star(\mathbf{r})\}, \qquad (2)$$

where $\mathbf{j}(\mathbf{r})$ and $\mathbf{E}(\mathbf{r})$ are the complex amplitudes of the electronic current density and the electric field. The relations $\mathbf{j}(\mathbf{r}) = i\omega\mathbf{P}(\mathbf{r})$ and $\mathbf{P}(\mathbf{r}) = \varepsilon_0(\varepsilon_\omega - 1)\mathbf{E}(\mathbf{r})$ permit us to express the HSD as a function of the electric field from the previous equation:

$$h(\mathbf{r}) = \omega\varepsilon_0 \, \mathrm{Im}(\varepsilon_\omega)|\mathbf{E}(\mathbf{r})|^2, \qquad (3)$$
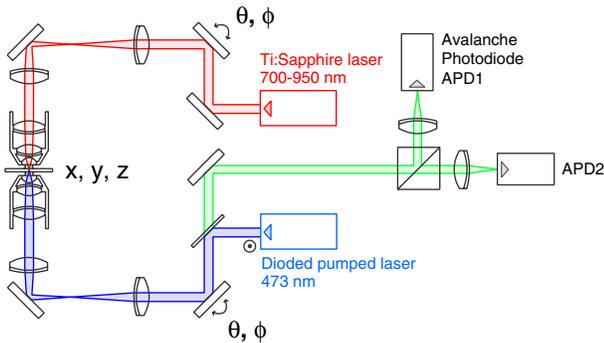

FIG. 1 (color online). Schematic view of the experimental setup.

where ω is the angular frequency of light and ε_ω is the permittivity of the metal [18]. Using the Green function formalism, the general solution of the temperature profile inside the structure can be written as

$$T(\mathbf{r}) = \int_V G(\mathbf{r}, \mathbf{r}')h(\mathbf{r}')d\mathbf{r}', \qquad (4)$$

where the integral runs over the structure volume V, $G(\mathbf{r}, \mathbf{r}')$ is the scalar thermal Green function associated to the Poisson equation (1) that vanishes at infinity. Similarly, using the Green dyadic formalism of electrodynamics [19,20], the electric field amplitude inside the structure reads:

$$\mathbf{E}(\mathbf{r}) = \int_V \mathcal{K}(\mathbf{r}, \mathbf{r}') \cdot \mathbf{E}_0(\mathbf{r}')d\mathbf{r}', \qquad (5)$$

where $\mathcal{K}(\mathbf{r}, \mathbf{r}')$ is the generalized Green dyadic tensor related to the plasmonic structure and $\mathbf{E}_0(\mathbf{r})$ is the external field exciting the structure. Under plane wave illumination, $\mathbf{E}_0(\mathbf{r}) = E_0\mathbf{u}_x$, where $\mathbf{u}_x$ is the unit vector along the x axis. From Eqs. (4) and (5) and after introducing the complex vector $\mathcal{K}(\mathbf{r}, \mathbf{r}') \cdot \mathbf{u}_x = \mathbf{K}_x(\mathbf{r}, \mathbf{r}')$, the HSD distribution generated by a plane wave illumination is given by

$$h_{\mathrm{PW}}(\mathbf{r}) = \omega\varepsilon_0 \, \mathrm{Im}(\varepsilon_\omega)E_0^2 \left| \int_V \mathbf{K}_x(\mathbf{r}, \mathbf{r}')d\mathbf{r}' \right|^2. \qquad (6)$$

In practice this HSD cannot be directly measured under plane wave illumination but by scanning a finite-size light spot, as explained above. Let us consider this light spot as a Dirac distribution field located in $\mathbf{r}_0$ and defined by $\mathbf{E}_0(\mathbf{r}) = vE_0\mathbf{u}_x\delta(\mathbf{r} - \mathbf{r}_0)$, where v has dimensions of volume and can be incorporated in the volume of excitation. The temperature distribution generated by such a local excitation reads then:

$$T_{\mathrm{loc}}(\mathbf{r}) = v^2E_0^2 \int_V \omega\varepsilon_0 \, \mathrm{Im}(\varepsilon_\omega)G(\mathbf{r}, \mathbf{r}')|\mathbf{K}_x(\mathbf{r}', \mathbf{r}_0)|^2d\mathbf{r}'. \qquad (7)$$

This exact solution can be simplified using two approximations. First, as mentioned above, even under local excitation, temperature processes at the submicrometric scale are so fast that the temperature remains quasiuniform. As a consequence, $G(\mathbf{r}, \mathbf{r}')$ behaves as a constant G_0, and $T(\mathbf{r})$ can be reduced to $T(\mathbf{r}_0)$. In addition, after applying a mean field approximation [21] on the volume V of the structure to perform the spatial integrals of $\mathbf{K}_x(\mathbf{r}, \mathbf{r}')$ and $\mathbf{K}_x(\mathbf{r}', \mathbf{r}_0)$, Eqs. (6) and (7) can be rewritten as

$$h_{\mathrm{PW}}(\mathbf{r}) = \omega\varepsilon_0 \, \mathrm{Im}(\varepsilon_\omega)V^2E_0^2\overline{|\mathbf{K}_x(\mathbf{r})|^2}, \qquad (8)$$

$$T_{\mathrm{loc}}(\mathbf{r_0}) = v^2E_0^2VG_0\omega\varepsilon_0 \, \mathrm{Im}(\varepsilon_\omega)\overline{|\mathbf{K}_x(\mathbf{r}_0)|^2}, \qquad (9)$$

leading to a linear relation between the HSD $h_{\mathrm{PW}}(\mathbf{r})$ obtained under plane wave illumination—the quantity we want to measure—and the temperature $T_{\mathrm{loc}}(\mathbf{r})$ measurement under local illumination—the quantity we actually record in our experiment:

$$h_{PW}(\mathbf{r}) = T_{loc}(\mathbf{r}) \frac{V}{v^2 G_0}. \qquad (10)$$

Figure 2 illustrates the two operational modes of the technique on a gold nanowire. Figure 2(a) shows the experimental measurement of the steady-state temperature distribution $T(\mathbf{r})$ around the gold structure while Figs. 2(b) and 2(c) give the associated distribution of the HSD $h(\mathbf{r})$ for both parallel and perpendicular polarizations. As expected, while the temperature spreads out of the nanowire, the heat origin is restricted to the metal. While this first example is meant only to introduce the two quantities that can be measured [$T(\mathbf{r})$ and $h(\mathbf{r})$], it is already a first indication of the counterintuitive physics of the HSD $h(\mathbf{r})$: for a transverse polarization of the incident light [Fig. 2(c)], the heat arises mainly from the extremities, while the optical near-field enhancement is expected at these locations precisely for the other polarization.

In order to understand this unexpected behavior and get further insight into the physics of photoinduced heat generation in plasmonic nanostructures, we study in detail a nanoantenna geometry consisting of two adjacent gold nanorods [Fig. 3(a)]. This structure features a longitudinal $3\lambda/2$ localized plasmon resonance centered at 850 nm [Fig. 3(b)]. The optical near-field properties of this structure have been extensively investigated in a previous work using TPL microspectroscopy [22] where we showed that the TPL distribution can be directly compared to the near-field distribution of $|E|^4$. HSD measurements for both incident polarizations are presented in Figs. 3(c) and 3(d) and compared to TPL measurements [Figs. 3(e) and 3(f)]. While under longitudinal polarization a strong optical field concentration and enhancement is observed within the gap region [Fig. 3(e)]; interestingly, the HSD behaves just the opposite way [Figs. 3(c) and 3(d)]. Associated numerical simulations of the $|E|^4$ distribution and of the HSD

[Figs. 3(g)–3(j)] support well our experimental measurements. Numerical simulations of charge [23] and current densities are displayed in Figs. 3(k)–3(n) to bring some further understanding: Optical hot spots usually come from tip effect and charge accumulation at the metal inter-
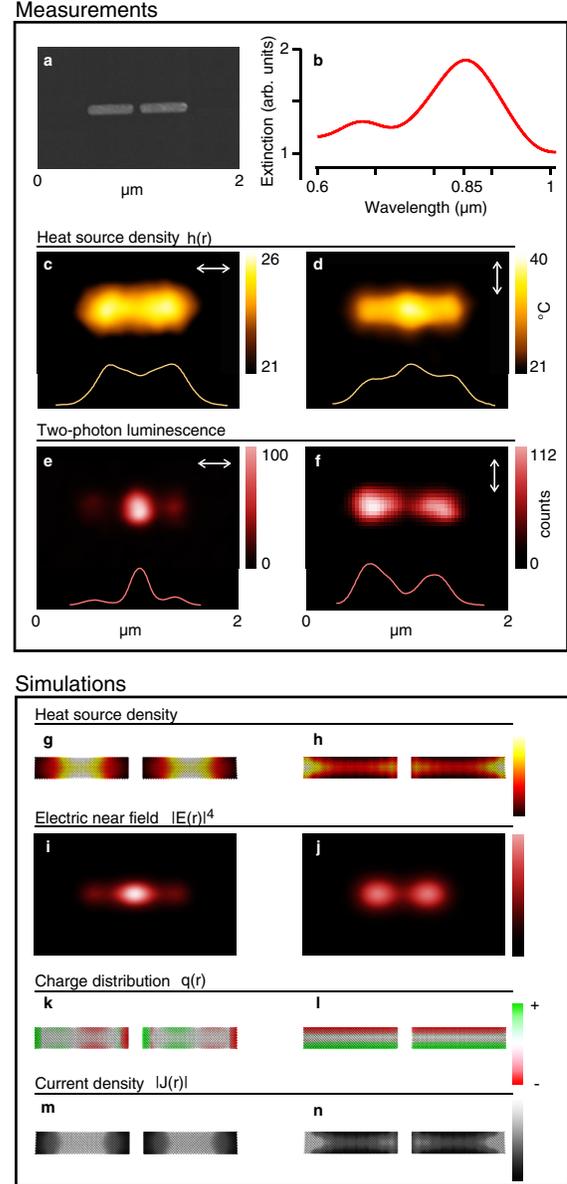
FIG. 3 (color online). Scanning electron microscopy (SEM) image (a) representing the structure of interest that consists of two rods (460 nm long, 100 nm wide, and 40 nm thick) separated by a gap of 60 nm. (b) Experimental extinction spectrum showing the longitudinal resonance at 850 μm. HSD maps for horizontal (c) and vertical (d) polarizations of the incident light ($P = 3.5$ mW, $\lambda = 850$ nm). Two-photon luminescence maps for horizontal (e) and vertical (f) polarizations of the incident light ($P = 76$ μW, $\lambda = 850$ nm). Associated numerical simulations using the Green dyadic tensor technique on a structure composed of 8926 cells: heat source density (g),(h), electric near field (i),(j), charge distribution (k),(l), and current density distribution (m),(n).
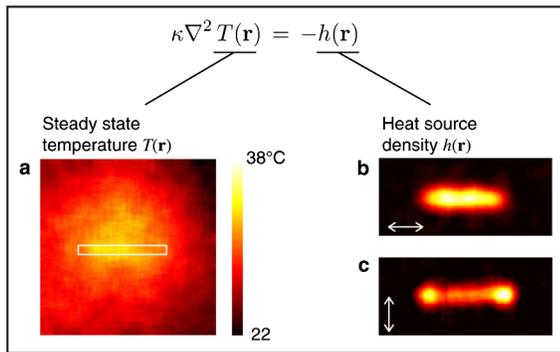

FIG. 2 (color online). (a) Steady state temperature profile measured around a gold nanowire lying upon a glass substrate (the wire is 200 nm wide, 35 nm thick, and 2 μm long). (b), (c) Experimental measurements of the associated heat source density for (b) a light parallel and (c) perpendicular to the nanowire axis This polarization is represented by the white double arrows. The laser wavelength is 725 nm and the illuminance around 40 mW/μm^2.
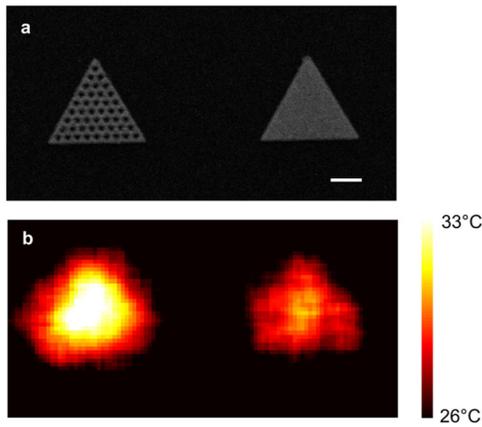
FIG. 4 (color online). SEM image of two gold triangles (a) 35 nm thick. The right triangle is characterized by a nanohole pattern. Experimental measurement of the HSD (b) showing a higher HSD associated with the nanostructured triangle (scalebar: 500 nm).

face [Figs. 3(k) and 3(l)], whereas heat arises on the contrary from areas where charges can freely flow [Figs. 3(m) and 3(n)]. This particular example evidences a general rule: In plasmonic structures, the heat origin does not usually match the optical hot spots. Note that TPL and HSD measurements appear thus as complementary techniques to understand where the energy of a plasmonic mode is optically and thermally released into the surroundings.

The method we present is not restricted to sharply resonant plasmonic nanoparticles. As an application of our method, we show how HSD measurements can help to design more efficient nanosources of heat in general. Using e-beam lithography, we have designed mesoscopic structures patterned with a lattice of nanoholes (Fig. 4). In this particular case, we observe that the heat generation is increased by around 40%—while the amount of gold is actually reduced by a factor of 2. A substantial optimization is achieved by increasing the amount of interfaces to generate electronic current everywhere inside the structures and not only at the outer boundaries. Because of its complexity, such a nanostructuration remains difficult to investigate numerically, while the experimental technique we present in this Letter has no limitation concerning the complexity of the system. This new kind of nanostructuration enables us to reduce the required heating laser power to achieve the desired temperature and could have applications in thermal-induced heterogeneous catalysis of chemical reactions at the nanometer scale where the surface/volume aspect ratio is known to be the important parameter.

*guillaume.baffou@icfo.es
†romain.quidant@icfo.es

[1] L. Cao, D. Barsic, A. Guichard, and M. Brongersma, Nano Lett. **7**, 3523 (2007).

[2] W. A. Challener, C. Peng, A. V. Itagi, D. Karns, W. Peng, Y. Peng, X. M. Yang, X. Zhu, N. J. Gokemeijer, Y.-T. Hsia, G. Ju, R. E. Rottmayer, M. A. Seigler, and E. C. Gage, Nat. Photon. **3**, 220 (2009).

[3] G. L. Liu, J. Kim, Y. Lu, and L. P. Lee, Nature Mater. **5**, 27 (2006).

[4] V. Garces-Chavez, R. Quidant, P. J. Reece, G. Badenes, L. Torner, and K. Dholakia, Phys. Rev. B **73**, 085417 (2006).

[5] X. Miao, B. K. Wilson, and L. Y. Lin, Appl. Phys. Lett. **92**, 124108 (2008).

[6] L. Wang and B. Li, Phys. Rev. Lett. **101**, 267203 (2008).

[7] L. Wang and B. Li, Phys. Rev. Lett. **99**, 177208 (2007).

[8] S. Lal, S. E. Clare, and N. J. Halas, Acc. Chem. Res. **41**, 1842 (2008).

[9] A. M. Gobin, M. H. Lee, N. J. Halas, W. D. James, R. A. Drezek, and J. L. West, Nano Lett. **7**, 1929 (2007).

[10] P. K. Jain, I. H. El-Sayed, and M. A. El-Sayed, Nano Today **2**, 18 (2007).

[11] G. Han, P. Ghosh, M. De, and V. M. Rotello, NanoBiotechnology **3**, 40 (2007).

[12] Y. de Wilde, F. Formanek, R. Carminati, B. Gralak, P. A. Lemoine, K. Joulain, J. P. Mulet, Y. Chen, and J. J. Greffet, Nature (London) **444**, 740 (2006).

[13] G. Domingues, S. Volz, K. Joulain, and J. J. Greffet, Phys. Rev. Lett. **94**, 085901 (2005).

[14] E. Rousseau, A. Siria, G. Jourdan, S. Volz, F. Comin, J. Chevrier, and J. J. Greffet, Nat. Photon. **3**, 514 (2009).

[15] A. O. Govorov and H. H. Richardson, Nano Today **2**, 30 (2007).

[16] G. Baffou, R. Quidant, and C. Girard, Appl. Phys. Lett. **94**, 153109 (2009).

[17] G. Baffou, M. P. Kreuzer, F. Kulzer, and R. Quidant, Opt. Express **17**, 3291 (2009).

[18] P. B. Johnson and R. W. Christy, Phys. Rev. B **6**, 4370 (1972).

[19] O. J. F. Martin, C. Girard, and A. Dereux, Phys. Rev. Lett. **74**, 526 (1995).

[20] C. Girard, E. Dujardin, G. Baffou, and R. Quidant, New J. Phys. **10**, 105016 (2008).

[21] This mean field approximation amounts to assimilating $\int |\mathbf{K}_x(\mathbf{r}', \mathbf{r}_0)|^2 d\mathbf{r}'$ and $|\int \mathbf{K}_x(\mathbf{r}', \mathbf{r}_0) d\mathbf{r}'|^2$. This working hypothesis is justified by the agreement with the experimental data. However, such an approximation loses validity when considering symmetric (with respect to the charge distribution, e.g., "+ − +") modes since they cannot be excited using a plane wave, while they can be excited by using a focused beam. In such a case, h_{PW} equals zero while t_{loc} does not.

[22] P. Ghenuche, S. Cherukulappurath, T. H. Taminiau, N. F. van Hulst, and R. Quidant, Phys. Rev. Lett. **101**, 116805 (2008).

[23] R. Marty, G. Baffou, A. Arbouet, C. Girard, and R. Quidant, Opt. Express **18**, 3035 (2010).